**EREM 80/4**
Journal of Environmental Research, Engineering and Management
Vol. 80 / No. 4 / 2024
pp. 60–74
10.5755/j01.erem.80.4.37407

**Mapping Land Use and Assessing Coastal Urbanization Impacts: A Case Study in Tangier Northern Morocco**

Received 2024/05 | Accepted after revisions 2024/08

**https://doi.org/10.5755/j01.erem.80.4.37407**

# Mapping Land Use and Assessing Coastal Urbanization Impacts: A Case Study in Tangier Northern Morocco

**Ali Hadek*, Miriam Wahbi, Boutaina Sebbah, Mustapha Maatouk, Hakim Boulaassal, Omar El Kharki, Otman Yazidi Alaoui**

Laboratory of Research and Development in Applied Geosciences, FSTT, Abdelmalek Essaadi University, Morocco

***Corresponding author:** ali.hadek@etu.uae.ac.ma

Tangier, one of Morocco's largest coastal cities strategically located between two maritime boundaries, has undergone significant transformations, particularly through the revitalization of its port area, leading to the establishment of a coastal path and waterfront. Given this context, conducting large-scale, precise spatiotemporal analysis and land-use classification is crucial for fostering Tangier's sustainable development. In this paper, a random forest algorithm was utilized to map land use changes in Tangier city using Landsat images, which has led to the generation of land use maps of the city from 2000 to 2023. The results show high accuracy in identifying land-use classes with an overall accuracy of 96% and a kappa coefficient exceeding 0.96. Moreover, the spatiotemporal analysis revealed notable changes: built-up land and forested areas increased by 124.55% and 41.11%, respectively, while maritime water areas decreased by 5%, and vegetation areas experienced a 30% decrease, on the other hand. The techniques presented in this study contribute to enhancing the precision of land-use classification within the complex environment of Tangier. They provide valuable technical support for conducting natural resource surveys and promoting sustainable regional development in the city.

**Keywords:** Tangier, land use change, remote sensing, random forest, sustainable urban planning.

## Introduction

Understanding the long-term dynamics of land use and land cover (LULC) is a fundamental strategy for quantifying gradual changes in the environment, managing natural resources, and planning for sustainable development. This comprehension plays a crucial role in various domains, including water management, agriculture, combating desertification and mitigating climate change (Mushtaq et al., 2022). The primary

driver of environmental changes is the alterations of land use and land cover resulting from human activities and their interactions with the environment. These alterations are influenced by various factors, including population growth, environmental exploitation, urbanization, deforestation, tourism development activities, improper land use, and anthropogenic actions (Lambin et al., 2001). These factors shape and transform the current landscape of land use and land cover (Jaiswal et al., 1999; Yuan et al., 2005; Sharma and Joshi, 2013; Rawat and Kumar, 2015). Therefore, accurate and reliable information regarding land cover changes and area expansion is fundamental for the development of effective land-use policies and environment protection by decision-makers, government agencies, and investors (Camalan et al., 2022; Becker et al., 2021; Mousa et al., 2020). Satellite data dedicated to land resources prove to be of paramount importance for detecting land use/cover changes (Yuan et al., 2005). The literature highlights Landsat satellite optical imagery with its different sensors (i.e., MSS, TM, and ETM+) as the most utilized image set (Amani et al., 2020), representing valuable and continuous records of the Earth's surface over the past three decades. These images, with their adequate spectral properties, provide better information on LULC changes compared with point data collected by on-site instruments during in-situ surveys (Muttitanon and Tripathi, 2005).

The integration of remote sensing technologies and geographic information systems has demonstrated remarkable efficiency in mapping and evaluating urban land use changes (Phan et al., 2020). This provides a detailed and cost-effective approach for regional land allocation across agricultural, urban, and industrial areas (Reis et al., 2003; Setti et al., 2020). These technologies enable continuous observation of the Earth's surface, creating vast databases that can be used to generate land use maps and detect dynamic changes and transformations with improved accuracy and efficiency (Singh, 1989; Lu et al., 2005; Sbai et al., 2016; Kolli et al., 2020). Precise LULC maps play a crucial role in classifying land into major categories, providing an overview of resources, their utilization, and their impact on socio-economic development (Betts et al., 2003; Griffith et al., 2003). Capital methodological approaches exist for exploiting satellite imagery to obtain accurate maps. Among these, multi-temporal land use analysis is one of the most widely used methods, due to its ability to consider spatial distribution. Today, modern remote sensing technologies benefit from the emergence and development of cloud storage and cloud computing platforms, such as Google Earth Engine (GEE), which offers powerful support tools to monitor and analyze environmental characteristics at a large scale. GEE includes numerous satellite datasets with general classification algorithms such as random forest (RF), widely employed for land cover mapping (Gislason et al., 2006; Rodriguez-Galiano et al., 2012a; Gorelick et al., 2017). RF improves LULC mapping accuracy compared with other prominent comparable methods (Zeferino et al., 2020). This algorithm offers high classification accuracy, is capable of handling high-latitude data, and eliminates the requirement for feature selection (Belgiu and Drăguț, 2016). The present study aims to utilize satellite imagery for a diachronic study of land use in Tangier, establishing its evolution and detecting changes over 23 years using the RF algorithm for classification (Mas, 2000; Lu et al., 2005). Land use maps are then used to extract artificial areas along the coastal fringe to study the evolution of urban areas in these zones, and to evaluate the impact of land use development on the coastal area. In this article, we examine the random forest algorithm on Google Engine. The structure of the document is as follows. Section 2 describes the Materials and Methods applied to the study area and presents the datasets and accuracy evaluation. Section 3 provides the Results and Discussion, including various LULC maps of Tangier. We evaluate the performance of the random forest algorithm using confusion matrices and calculate the kappa index, followed by an examination of the spatiotemporal changes. Section 4 presents a discussion of the results and concludes the study.

## Materials and Methods

### Study area

The Tangier region, an integral part of the western sector of the Moroccan Mediterranean, is composed of a series of low plains, the most significant of which is the Fahs plain, frequently traversed by several streams. This area is bordered by prominent highlands such as the Malabata and Spartel capes, the Jbel Lkbir and Jbel Zhirou mountains, and is dominated to the east by the Internal Rif Limestone Chain (Ait Brahim et al., 2018; Mamouni et al., 2019). Geographically, Tangier covers

an area of 1195 km², with longitude ranging from 5°33'W to 6°05'W, and latitude from 35°19'N to 35°51'N (*Fig. 1*). Positioned on the Strait of Gibraltar, Tangier is the only Moroccan city that has two sea fronts. it is bounded to the north by the Strait of Gibraltar, to the west by the Atlantic Ocean, to the south by the city of Asilah, and to the east by the Paleozoic formations of the Internal Rif near Tetouan. This region belongs to the external domain of the Rif chain, specifically its northwestern part, and is characterized by the stacking of four flysch nappes resting on the Tangier unit: Mellousa, Béni Ider, Tisirène, and Numidian. The Tangier region is marked by a morphostructural context with significant structural control, tectonic and neotectonic activity affecting the entire region, giving rise to intense fracturing (Mamouni et al., 2019). Moreover, at the end of the last century, the Rif Mountains of Morocco have experienced significant changes at the level of agricultural activity, especially concerning the increase in cannabis cultivation characterized by high water requirements (Hmamou and Bounakaya, 2020).

Tangier features a Mediterranean climate, influenced by the nearby ocean, characterized as sub-humid with an average annual precipitation of 700 mm. Rainfall is predominant during the winter season, with a dry period extending from May to October. The average annual temperature stands at 17.5°C, with a mean maximum of 28.3°C and a mean minimum of 9°C (Imane et al., 2019). The city is divided into four urban districts and six rural communes. However, in our study area, we also include the urban district of Gzenaya. This addition aligns with the strategic goals outlined in the development plan for the Northern region, which prioritizes establishing significant inland urban centers to alleviate coastal congestion. Given its geographic location, Gzenaya with its industrial zone contributes significantly to forming a robust industrial center around the airport, positioned at the southern entrance to Tangier.

**Fig. 1.** *Localization of the study area*

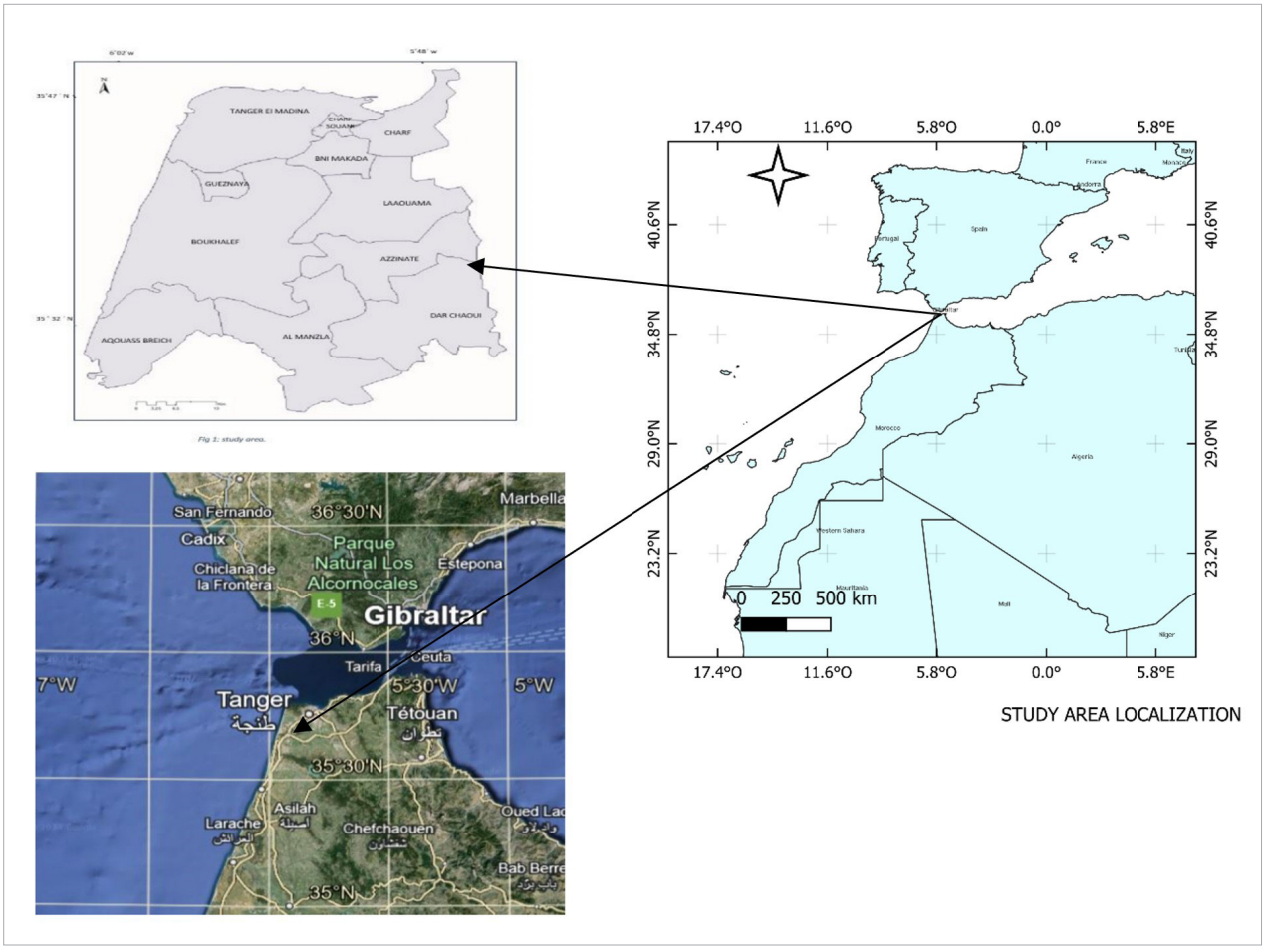

**Table 1.** *Landsat data used in this study*

| | Image 1 | Image 2 | Image 3 | Image 4 |
|---|---|---|---|---|
| Satellite | Landsat5/7 | Landsat5/7 | Landsat7/8 | Landsat7/8 |
| Acquisition period | 01/01/2000–30/05/2000 | 01/01/2008–30/05/2008 | 01/01/2015–30/05/2015 | 01/01/2023–30/05/2023 |
| Sensor | TM/ETM+ | TM/ETM+ | ETM+/OLI/TIRS | ETM+/OLI/TIRS |
| Mode | Multispectral | Multispectral | Multispectral | Multispectral |

## Datasets

This study utilized Landsat surface reflectance to analyze LULC, from Landsat 5 (TM), Landsat 7 (ETM+), and Landsat 8 (OLI) sensors, with data from the years 2000, 2008, 2015, and 2023 (*Table 1*). The year 2000 was selected to understand changes since the beginning of the century, following significant land acquisitions by companies and foreign individuals (Le Tellier, 2004). The year 2008 marks the midpoint of this period, reflecting the clear impact of climate change on temperature and precipitation trends in Tangier (Driouech, 2010). In 2015, the major reconstruction works of the port were nearly completed, signifying significant infrastructural changes (SAPT, 2015). Finally, 2023 was chosen to maintain a consistent interval due to the availability of high-quality Landsat images for accurate analysis. These data have been atmospherically corrected, and a cloud mask was used for cloud shadow and cloud-cover correction. Each data is selected with a cloud cover criterion of < 10% for each year. A series of key dates were selected to conduct this historical study. All selected satellite data were calculated for the median image of each study year, which was clipped to the study area boundary. The city's spatial growth began in the early 21$^{st}$ century through land acquisitions by foreign companies and individuals. The first selected date was 2000 to understand changes that occurred in the city since the beginning of the century.

## Methodology

This study develops a method of the RF algorithm to extract land use and cover change in the study area. The classification and accuracy validation methods were implemented in a single Google Earth Engine (GEE) script, and the surface reflectance of Landsat data covering the study area was selected, and cloud cover was effectively masked. The classification involves a pixel-based technique, using the same training data and the random forest (RF) algorithm to obtain results. LULC extraction based on the RF method according to the actual situation of the land use in the study area involved seven land use categories (*Table 2*): Marine waters, Forest, Artificial territories, Vegetation, Continental water, Sand and dune, and Bare soil. A confusion matrix was generated by applying the random forest classifier to both the training and validation data. Additionally, visual interpretation was used to differentiate between land and water bodies. Following this, the change characteristics of each land use type were analyzed, with a focus on spatial patterns and temporal trends, to clarify the conversions between different land use types (Gislason et al., 2006; Tatsumi et al., 2015). Land use mapping is generally relying on multispectral classification methods, but other methods involve the application of remote sensing (Xu, 2008). To better distinguish objects and reduce class confusion, we chose to calculate new bands from the original bands of pre-processed images. These new bands correspond to the main land use classes, namely: vegetation through the calculation of the NDVI (Huang et al., 2021; Jiang, 2007), water via the MNDWI (2) (Xu, 2008) (*Fig. 3*). The ultimate goal of classification is to establish a correspondence between spectral classes and information classes (*Fig. 2*).

**Table 2.** *Classification category*

| Type | Description |
|---|---|
| Maritime water | Seas, Oceans, Water |
| Forest | Trees, Dense Vegetation |
| Artificial territories | Urban, Commercial, Infrastructure |
| Continental waters | Lakes, Dams, Waterways |
| Vegetation | Crops, Urban Parks |
| Sand and dune | Beach, Sand, Valleys |
| Bare soils | Exposed, Unvegetated, Ground |

**Fig. 2.** *Flowchart of this study*

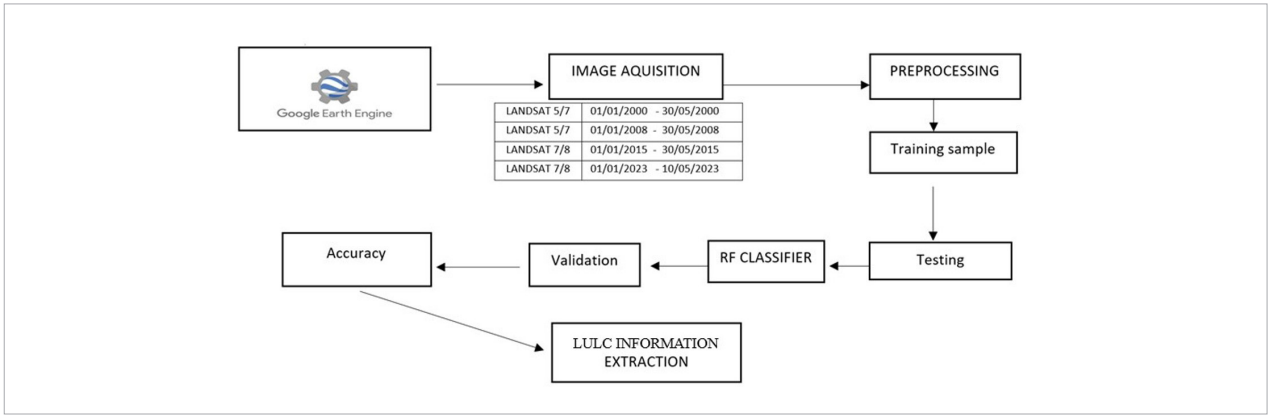


### Classifier construction based on the RF algorithm

The random forest (RF), a machine learning classifier derived from decision trees, has emerged as a favored and highly promising choice among learners for its consistent and resilient classification accuracy. The RF classifier in Google Earth Engine had a strong performance with overall classification accuracy ≥ 0.96 and a kappa coefficient ≥ 0.93 using Landsat imagery (Kadri et al., 2023; Srivastava et al., 2019). Its efficacy in managing vast, high-dimensional datasets has further cemented its popularity, making it a widely utilized tool in the classification of multi-temporal and multi-sensor images (Amini et al., 2022; Dhu et al., 2019; Bourgoin et al., 2020). RF was selected for this study because it produced almost accurate quality results for land use classification even when no hyperparameters were present. The random forest algorithm implemented within the GEE platform is a nonparametric regression method. It consists of a set of regression trees constructed from training data, usually a set of samples taken randomly from the original training set replacement. A regression tree is built for each bootstrap set, which together creates the RF. It is a series of rules used to split a feature space into partitions with similar response variable values (Chen et al., 2021). GEE is a cloud-based platform that supports the display, calculation, and analysis of global satellite imagery. Building a random forest classifier involves two main elements: random data and feature selection. The number of decision trees was set to 100, and other parameters were set to the default values. Regarding the sample points, 70% of them were used for classifier training, and the remaining 30% were used as out-of-bag samples for accuracy verification. Compared with other regression methods, RF has several advantages, thereby becoming an attractive regression tool. RF does not overfit when the number of regression trees increases and does not require variable selection.

### Accuracy evaluation

Accuracy assessment represents an essential procedure within the realm of remote sensing data extraction and target recognition, as it quantifies the similarity between the produced and reference maps. This assessment serves a dual purpose: firstly, to appraise the precision of the outcomes; and secondly, to establish a performance benchmark while optimizing associated parameters. In this study, the internal confusion matrix algorithm of GEE was employed to validate and assess the accuracy of image classification (Phan et al., 2020). The overarching accuracy, denoted as the overall accuracy (OA), quantifies the correctly classified pixels situated along the diagonal of the confusion matrix, serving as a direct indicator of accurate classification proportion. Furthermore, the kappa coefficient is employed to ascertain whether the model's predictive outcomes align with the actual classification results (Liu et al., 2007; Foody, 2002).

## Results and Discussion

### Assessing the performance of LULC for Tangier

The analysis of images for the years 2000, 2008, 2015, and 2023 enabled the establishment of land use maps for the Tangier region (*Fig. 4*; *Fig. 5*; *Fig. 6*; *Fig. 7*). Before embarking on the analysis and interpretation of these

maps, it is prudent to evaluate the classification results. This validation was carried out through visual comparison of the classification results with Google Earth images and ground truth data (Cheng et al., 2017; Khatami et al., 2017). The accuracy of the results is assessed based on the confusion matrix (*Table 4*, *Table 5*, *Table 6*, *Table 7*, respectively) presenting the matrices obtained for the selected images. The overall accuracy percentage and the kappa coefficient, as defined in Equation (2) for the four classifications are 96.6% and 0.92, respectively (*Table 3*). Consequently, these classifications are considered reliable and suitable for the area's interest.

**Table 3.** *Classification accuracy*

| Year | 2000 | 2008 | 2015 | 2023 | Average |
|---|---|---|---|---|---|
| **Kappa** | 0.93 | 0.83 | 0.97 | 0.96 | 0.92 |
| **OA** | 94.64% | 97.32% | 97.77% | 96.78% | 96.62% |

**Fig. 3.** *MNDWI 2000, 2008, 2015, 2023*

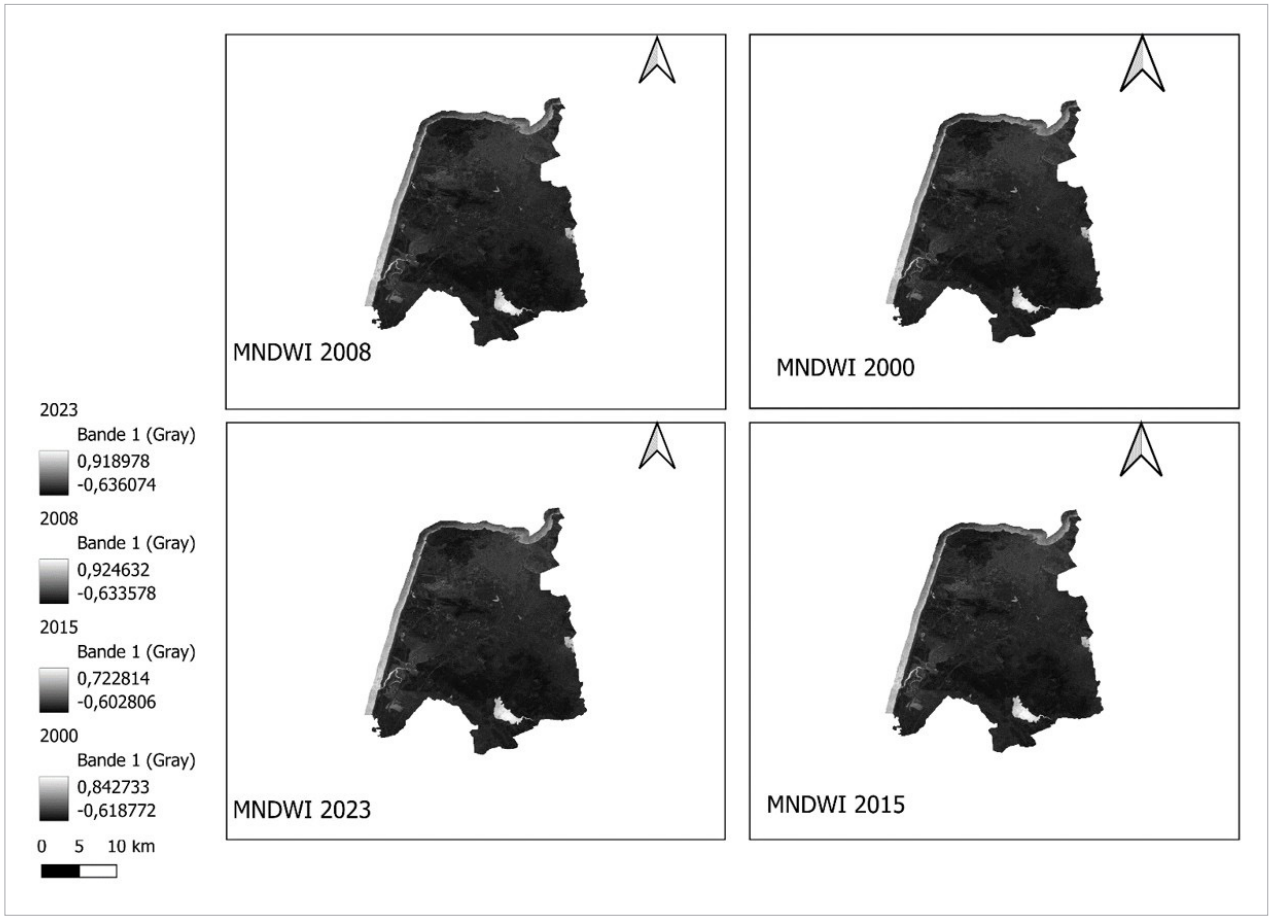


$$\text{MNDWI} = \frac{\text{Green} - \text{SWIR}}{Green + SWIR} \quad (1)$$

where SWIR refers to pixel values from the short-wave infrared band; and Green refers to pixel values from the green band.

$$\text{K} = \frac{\text{P0} - \text{Pe}}{1 - \text{pe}} \quad (2)$$

where $p_o$ is the observed agreement among raters or the proportion of instances where the classification matches the ground truth; and $p_e$ is the expected agreement by chance, calculated based on the distribution of each category.

**Fig. 4.** *Land use and land cover in 2000*

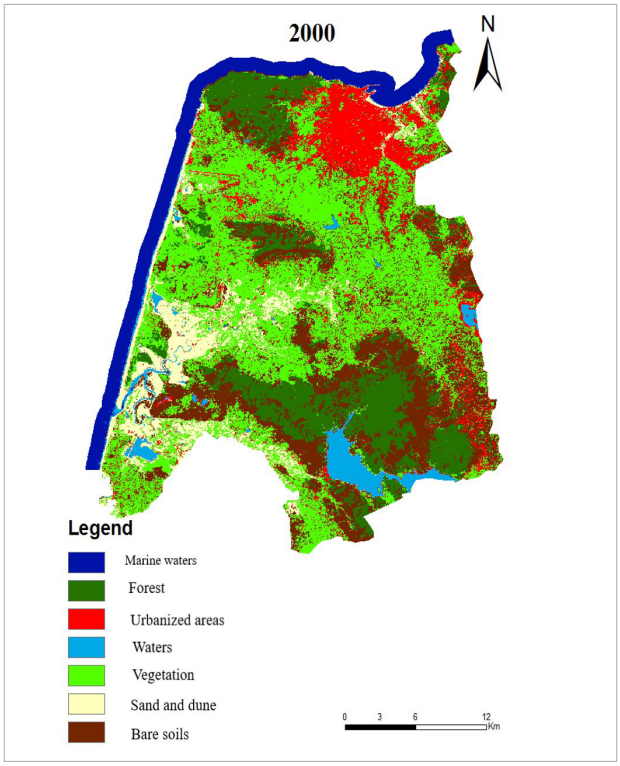


**Fig. 5.** *Land use and land cover in 2008*

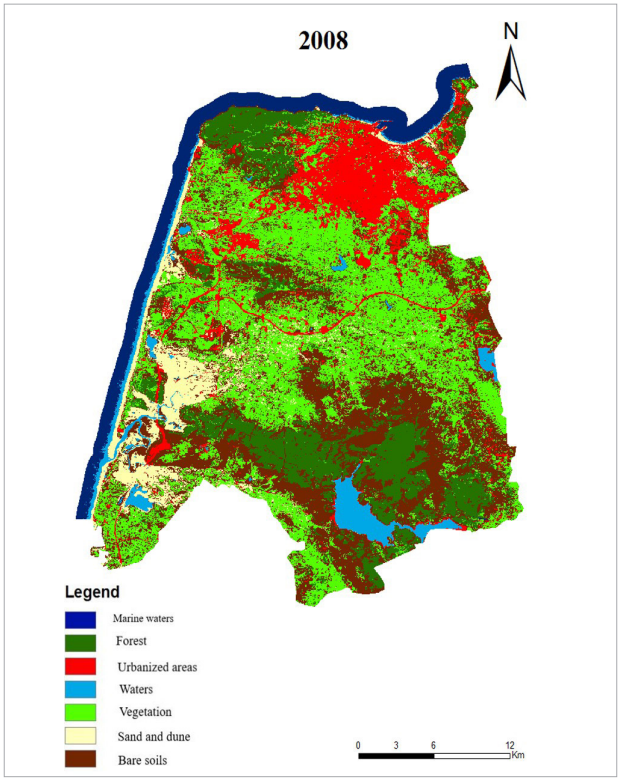


**Fig. 6.** *Land use and land cover in 2015*

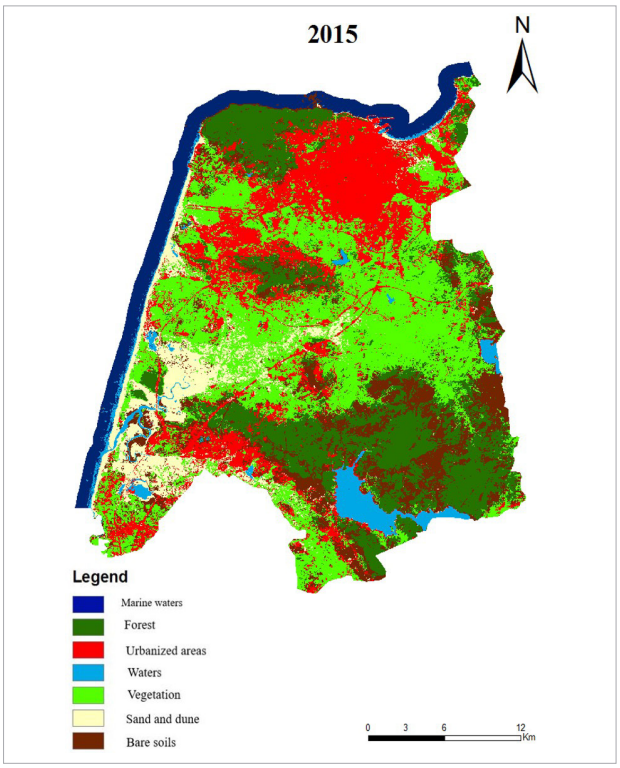


**Fig. 7.** *Land use and land cover in 2023*

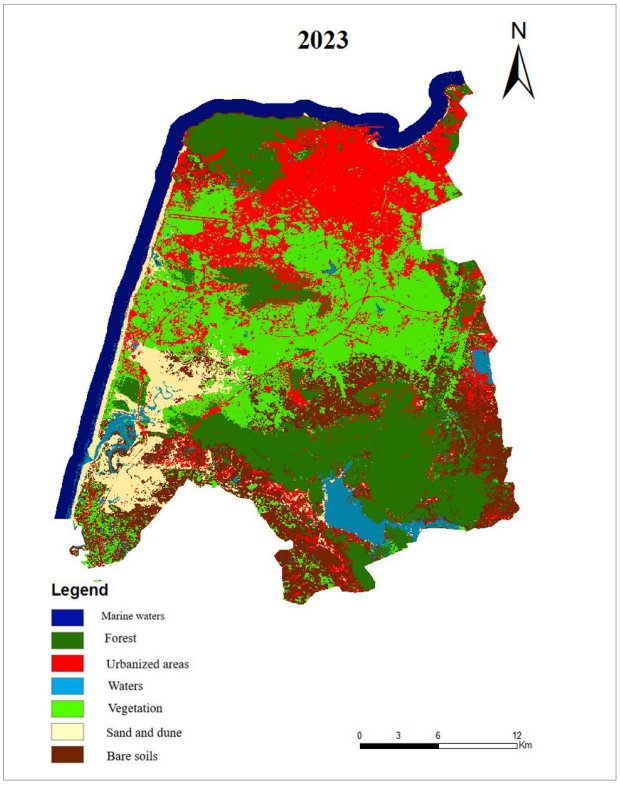

**Table 4.** *Confusion matrix for the image classification of 2000*

| Classification references | Maritime waters | Forest | Artificial territories | Continental waters | Vegetation | Sand dune | Bare soils | Total | Error commission | User accuracy % |
|---|---|---|---|---|---|---|---|---|---|---|
| **Maritime water** | 40 | 1 | 0 | 0 | 0 | 0 | 1 | 42 | 0.04 | 95.23 |
| **Forest** | 0 | 60 | 0 | 1 | 0 | 0 | 1 | 62 | 0.03 | 96.77 |
| **Artificial territories** | 1 | 1 | 23 | 0 | 1 | 0 | 0 | 26 | 0.11 | 88.46 |
| **Continental waters** | 0 | 0 | 1 | 34 | 0 | 0 | 1 | 36 | 0.05 | 94.44 |
| **Vegetation** | 0 | 0 | 1 | 0 | 32 | 1 | 0 | 34 | 0.05 | 94.11 |
| **Sand and dune** | 0 | 0 | 0 | 1 | 0 | 46 | 1 | 48 | 0.04 | 95.83 |
| **Bare soils** | 1 | 0 | 0 | 0 | 1 | 0 | 30 | 32 | 0.06 | 93.75 |
| **Total** | 42 | 62 | 25 | 36 | 34 | 47 | 34 | 280 | | |
| **Error omission** | 0.04 | 0.03 | 0.08 | 0.05 | 0.03 | 0.02 | 0.11 | | | |
| **Producer accuracy %** | 95.2 | 96.77 | 92 | 94.44 | 94.11 | 97.87 | 88.23 | | | |

**Table 5.** *Confusion matrix for the image classification of 2008*

| Classification references | Maritime waters | Forest | Artificial territories | Continental waters | Vegetation | Sand dune | Bare soils | Total | Error commission | User accuracy % |
|---|---|---|---|---|---|---|---|---|---|---|
| **Maritime water** | 10 | 1 | 0 | 0 | 0 | 0 | 0 | 11 | 0.09 | 90.90 |
| **Forest** | 0 | 40 | 0 | 0 | 0 | 0 | 1 | 41 | 0.02 | 97.56 |
| **Artificial territories** | 1 | 0 | 36 | 0 | 0 | 0 | 0 | 37 | 0.02 | 97.29 |
| **Continental waters** | 0 | 0 | 0 | 29 | 1 | 0 | 0 | 30 | 0.03 | 96.66 |
| **Vegetation** | 0 | 0 | 0 | 0 | 26 | 0 | 0 | 26 | 0 | 100 |
| **Sand and dune** | 0 | 0 | 0 | 0 | 0 | 37 | 0 | 37 | 0 | 100 |
| **Bare soils** | 0 | 0 | 1 | 0 | 0 | 1 | 40 | 42 | 0.04 | 95.23 |
| **Total** | 11 | 41 | 37 | 29 | 27 | 38 | 41 | 224 | | |
| **Error Omission** | 0.09 | 0.02 | 0.02 | 0 | 0.03 | 0.02 | 0.02 | | | |
| **Producer accuracy %** | 90.90 | 97.56 | 97.29 | 100 | 96.29 | 97.36 | 97.56 | | | |

**Table 6.** *Confusion matrix for the image classification of 2015*

| Classification references | Maritime waters | Forest | Artificial territories | Continental waters | Vegetation | Sand dune | Bare soils | Total | Error commission | User accuracy % |
|---|---|---|---|---|---|---|---|---|---|---|
| **Maritime water** | 10 | 0 | 1 | 0 | 0 | 0 | 0 | 11 | 0.09 | 90.90 |
| **Forest** | 1 | 43 | 0 | 1 | 0 | 0 | 0 | 45 | 0.04 | 95.5 |
| **Artifice territories** | 0 | 0 | 60 | 0 | 0 | 0 | 0 | 60 | 0 | 100 |
| **Continental waters** | 0 | 0 | 0 | 39 | 1 | 0 | 0 | 40 | 0.02 | 97.5 |
| **Vegetation** | 0 | 0 | 0 | 0 | 25 | 0 | 1 | 26 | 0.03 | 96.1 |
| **Sand and dune** | 0 | 0 | 0 | 0 | 0 | 55 | 1 | 56 | 0.01 | 83.3 |
| **Bare soils** | 0 | 0 | 0 | 0 | 0 | 0 | 32 | 32 | 0 | 95.23 |
| **Total** | 11 | 43 | 61 | 40 | 26 | 55 | 34 | 270 | | |
| **Error Omission** | 0.09 | 0 | 0.01 | 0.02 | 0.03 | 0 | 0.02 | | | |
| **Producer accuracy %** | 90.90 | 100 | 98.3 | 97.5 | 96.1 | 100 | 94.1 | | | |

**Table 7.** *Confusion matrix for the image of 2023*

| Classification references | Maritime waters | Forest | Artificial territories | Continental waters | Vegetation | Sand dune | Bare soils | Total | Error commission | User accuracy % |
|---|---|---|---|---|---|---|---|---|---|---|
| **Maritime water** | 18 | 1 | 0 | 0 | 0 | 0 | 0 | 19 | 0.05 | 90.90 |
| **Forest** | 0 | 46 | 0 | 1 | 0 | 0 | 0 | 47 | 0.02 | 95.5 |
| **Artifice territories** | 0 | 0 | 95 | 0 | 0 | 0 | 1 | 96 | 0.01 | 100 |
| **Continental waters** | 1 | 1 | 0 | 31 | 0 | 0 | 0 | 33 | 0.06 | 97.5 |
| **Vegetation** | 0 | 0 | 0 | 0 | 40 | 1 | 1 | 42 | 0.04 | 96.1 |
| **Sand and dune** | 0 | 0 | 0 | 0 | 1 | 47 | 0 | 48 | 0.02 | 83.3 |
| **Bare soils** | 0 | 0 | 0 | 1 | 1 | 0 | 24 | 26 | 0.07 | 95.23 |
| **Total** | 19 | 48 | 95 | 33 | 42 | 48 | 26 | 311 | | |
| **Error Omission** | 0.05 | 0.04 | 0 | 0.06 | 0.04 | 0.02 | 0.07 | | | |
| **Producer accuracy %** | 94.73 | 95.83 | 100 | 93.93 | 95.23 | 97.91 | 92.30 | | | |

## Examining the spatiotemporal changes in LULC in Tangier

In this study, the change characteristics of Maritime waters, Forests, Artificial territories, Continental waters, Vegetation, Sand and dune, and Bare soils were analyzed in terms of area change and area change rate (*Table 8*). The analysis of land occupation changes between 2000 and 2023 reveals notable trends. The area of marine water decreased from 52.91 km$^2$ to 50.15 km$^2$, showing a 5% reduction. Conversely, the forested area expanded from 109.33 km$^2$ in 2000 to 154.28 km$^2$ in 2023, marking a substantial 41.11% increase. Significant growth was also observed in artificial land, which increased from 69.23 km$^2$ to 155.46 km$^2$, indicating a significant 124.55% increase. Concerning continental water area, it has expanded from 23.21 km$^2$ to 25.36 km$^2$, representing a 9.26% increase. However, there was a notable decrease in vegetation area, which dropped from 260.44 km$^2$ to 180.70 km$^2$, reflecting a 30.61% decrease. Sand and dune area also decreased from 60.02 km$^2$ to 50.27 km$^2$, marking a 16.24% reduction. Finally, the bare land area decreased from 160.74 km$^2$ to 119.24 km$^2$, indicating a 24.81% reduction.

These changes highlight the dynamic shifts in the landscape over this period. The increase in forested land in the Tangier-Tetuan region can be attributed to the implementation of an extensive afforestation program by the Regional Directorate of Water and Forests and the Fight Against Desertification in the Rif during the 2014–2015 campaign. This program had a significant impact on the region's forested areas. Specifically, a total area of 2444 hectares was dedicated to tree planting to restore and preserve the local forests. Another reforestation project was initiated by the same department to regenerate the forest lost in a devastating fire that had swept through a part of the Cap Spartel forest in 2017. This initiative involves planting 267 000 trees over an area of approximately 265 hectares, to be achieved by 2023.

The increase in the urbanized area of nearly 86 km$^2$ over the past 23 years in Tanger can be attributed to several key factors. According to the 2014 population census, the population of Tangier has experienced an average annual growth of 3.08% since 2004. Moreover, it is essential to note that Tangier's prefectural urbanization rate was 94.3% in 2014, which is above the regional average of 59.9% and the national average of 60.4%. This high level of urbanization demonstrates that Tangier is becoming a major hub for urban development in Morocco. The prefecture of Tangier has witnessed the emergence of several significant urban centers, including the new city of Chrafate, aiming to produce 30 000 housing units, and the Ibn Battuta urban cluster, with plans for 16 000 housing units. The surface area of continental waters was estimated at 23 km$^2$ in 2000, a consequence of Morocco's significant warming trends between 1972 and 2004. This surface area has further increased compared with 2000, and this change depends not only on precipitation but also on the capturing of floodwaters by dams, particularly during the severe flooding incident witnessed by the city in 2008. The expansion of urbanized areas has led to a decrease in vegetation, sand, and bare soil. Tangier city is often

**Fig. 8.** *Land use distribution in 2000–2008*

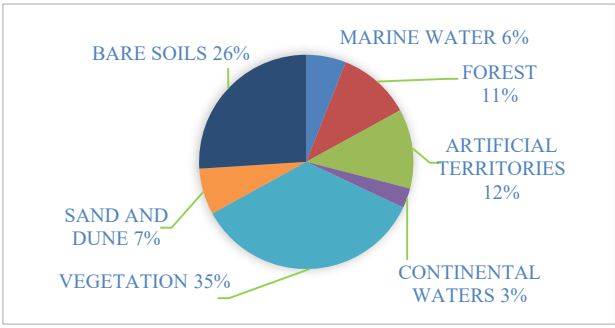


**Fig. 9.** *Land use distribution in 2008–2015*

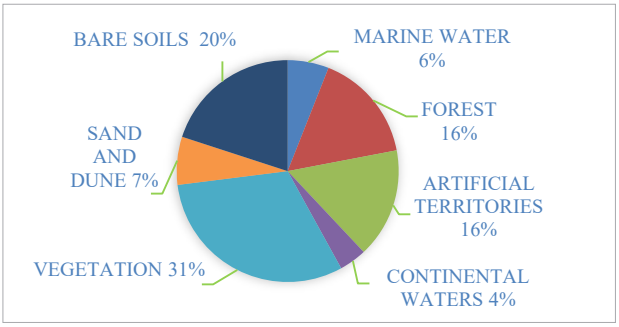


**Fig. 10.** *Land use distribution in 2015–2023*

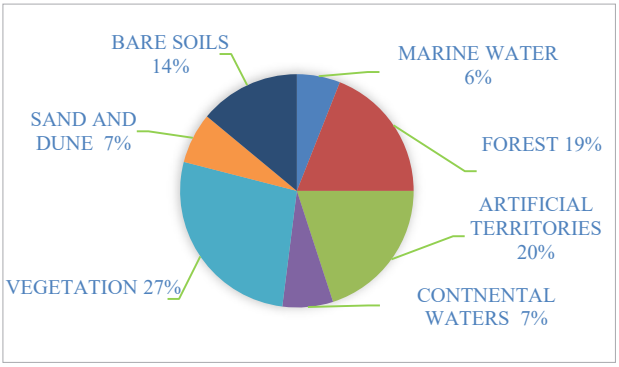


subject to meteorological disturbances, such as strong winds, severe thunderstorms, and heavy rainfall from mid-October to early May. However, the climatic effect on agricultural land can be neglected in this study, due to the absence of images captured during the rainy period (January to May).

The recorded variation rate in seawater area (5%) is almost negligible and can return to sea level at the time of image capture, likely influenced by tidal fluctuations (Bourouhou and Salmoun, 2021).

## Urban expansion of Tangier coastal zone

To estimate the coastal development degree, a distance of 10 kilometers was used, extending from the coastline towards the inland area (Wahbi et al., 2019), covering an approximate area of 95 km$^2$. Given that most of Tangier's coastlines are sandy, and urbanization typically occurs in these coastal areas, *Table 9* shows the percentage variations of these areas, while *Figs. 12–15* illustrate the evolution of urban development along the coastline. The total land gained during the observation period reached 30.03 km$^2$, indicating that approximately 1 305 652 m$^2$ of the coastline was transformed into urban areas annually throughout the study period. *Table 10* depicts the periods of urban expansion at the expense of the sea between 2000 and 2023.

Data analysis (*Figs. 8–10*) highlights that the first period (2000–2008) witnessed the lowest urban growth at the expense of the coastline, with only approximately 7.56 km$^2$ of land reclaimed, accounting for 25.2% of the total area. The period between 2008 and 2015 did not show a remarkable increase, with an estimated 9.57 km$^2$ of urbanized land. However, beyond 2015, it marked the most significant spatial expansion into the sea, where approximately 43% of the reclaimed land was developed between 2015 and 2023 (*Fig. 11*). During

**Table 8.** *Land use evolution of Tangier between 2000 and 2023*

| Land occupation | Area km$^2$ | | | | Variation % 2000/2023 |
|---|---|---|---|---|---|
| | 2000 | 2008 | 2015 | 2023 | |
| Marine water | 52.91 | 47.24 | 47.62 | 50.15 | –5 |
| Forest | 109.33 | 100.14 | 133.30 | 154.28 | 41.11 |
| Artificial land | 69.23 | 82.55 | 148.37 | 155.46 | 124.55 |
| Continental water | 23.21 | 26.38 | 25.21 | 25.36 | 9.26 |
| Vegetation | 260.44 | 230.24 | 224.72 | 180.70 | –30.61 |
| Sand and dune | 60.02 | 47.88 | 57.79 | 50.27 | –16.24 |
| Bare land | 160.74 | 201.41 | 97.66 | 119.24 | –24.81 |

**Table 9.** *The evolution of urban growth at the expense of the coastal areas between 2000 and 2023*

| Period | Area filled km² | Percentage % | Annual growth km² | Percentage% |
|---|---|---|---|---|
| 2000/2008 | 7.56 | 25.2 | 0.94 | 23.98 |
| 2008/2015 | 9.57 | 31.86 | 1.37 | 34.95 |
| 2015/2023 | 12.90 | 42.96 | 1.61 | 41.07 |
| Total | 30.03 | 100 | 3.92 | 100 |

**Table 10.** *Land use changes between 2000 and 2023 for the land artificialization and sand dune classes*

| Land use | Area km² | | | | Variation 2000/2023 |
|---|---|---|---|---|---|
| | 2000 | 2008 | 2015 | 2023 | |
| Artificial land | 7.3 | 7.82 | 11.31 | 14.50 | 98.63 |
| Sand and dune | 23.22 | 16.19 | 14.33 | 13.40 | –42.29 |

**Fig. 11.** *The variation in urbanization rates about sandy terrains between 2000 and 2023*

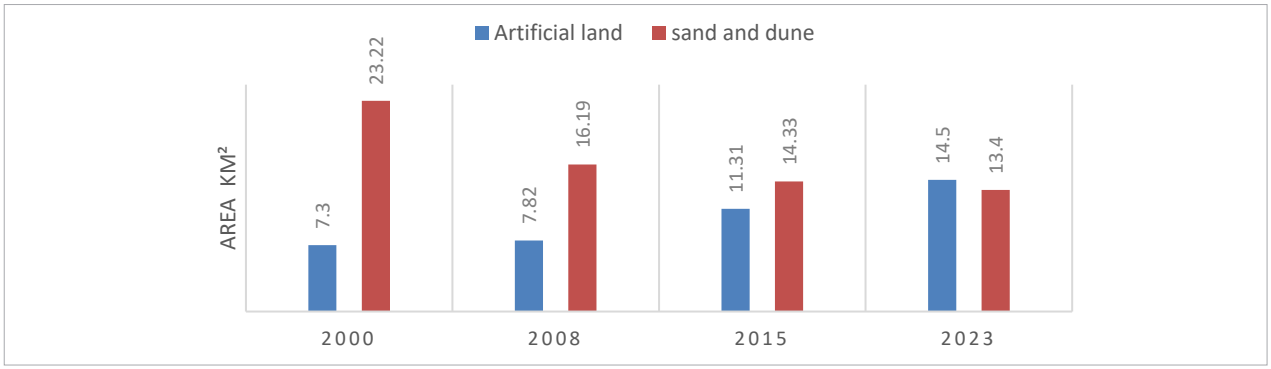


**Fig. 12.** *Coastal land lost to urban growth in 2000*

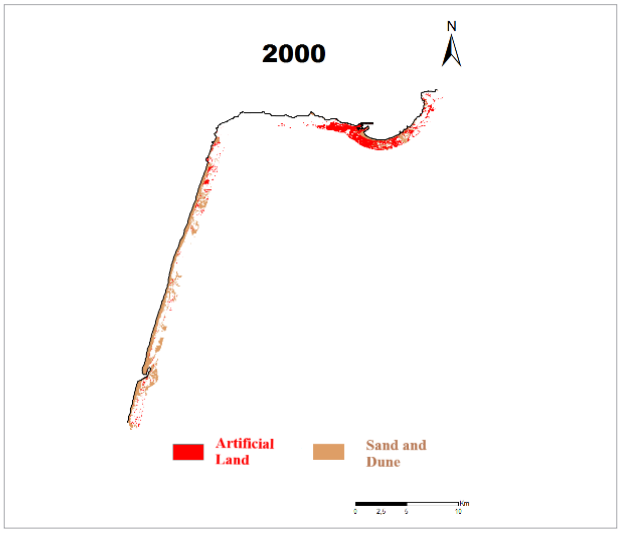


**Fig. 13.** *Coastal land lost to urban growth in 2008*

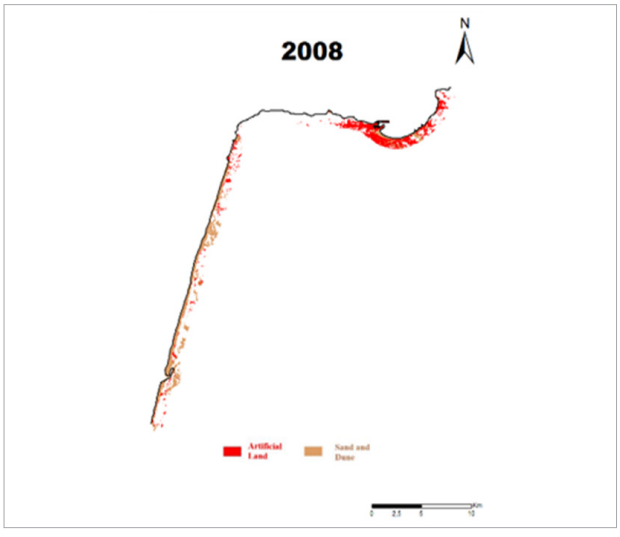

**Fig. 14.** *Coastal land lost to urban growth in 2015*

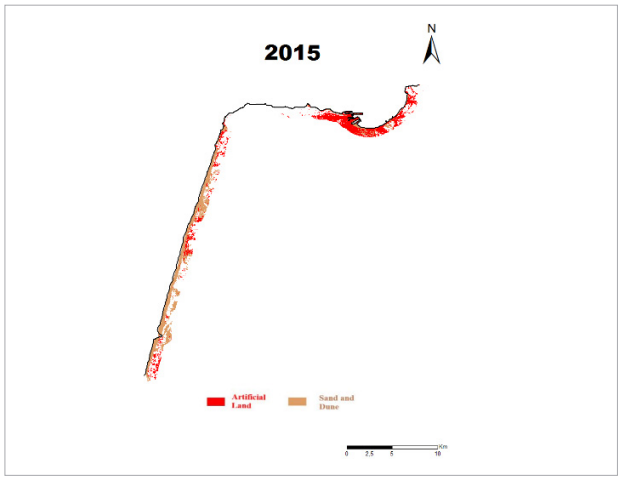


**Fig. 15.** *Coastal land lost to urban growth in 2023*

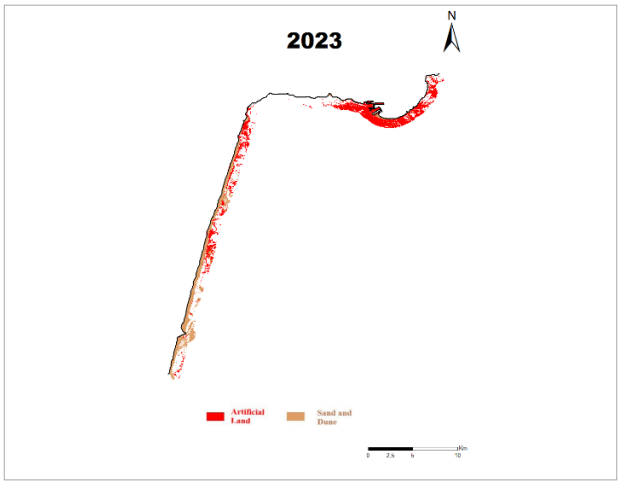


this period, the coastal zone lost 12.90 km$^2$ under the pressure of urbanization, with an average annual increase of 1.61 km$^2$/year.

### The evolution of the coastal urban landscape

The coastal landscape of Tangier has changed as land use patterns evolved, influenced by the socio-economic context and urban policies. In Tangier, the urban development around the bay has notably increased, driven mainly by the redevelopment of Tangier City Port. The port area has undergone significant expansion, growing from 160 ha in 2000 to a vast 84 000 m$^2$ by 2023. The conversion of the historic port began in 2011, contributing to the observed increase in urbanization between 2008 and 2015.

Along the coastal areas, various tourism projects have been established, such as the Ghandouri project in Tangier. This initiative has changed the bay's landscape by introducing luxurious accommodations like 5-star hotels, charming riads, and welcoming guesthouses. The Ghandouri development zone covers 60 hectares on the western edge of the bay, including an 18-ha forest, forming a sloping coastal strip that stretches over 1200 meters.

On the Atlantic coastline, different tourist and residential projects have been established along the shore. One significant project is the Al Houara Resort in Tangier, which was revealed in 2008. It covers an area of 234 hectares, including forests, wetlands, and sandy beaches. Al Houara Resort aimed to build three hotels, 15 villas, and around 180 apartments. The significant impact of this undertaking is evident in the land use map.

However, the Tangier Atlantic coastline has faced issues due to sand extraction, especially during the real estate boom in 1980 at Sidi Kacem Beach and in 1990 at Haoura Beach, which was stopped in 2006. This continuous extraction has increased the erosion risk for Tangier's sandy beaches. By the end of 2010, using satellite imagery, the Ministry of Equipment identified high-risk zones and classified beaches based on their level of degradation. The Tangier-Assilah beaches were ranked second among the most affected areas. Adding to these challenges, the Rocade des Deux Mers, a project initiated in Tangier by King Mohammed VI in 2014, aims to create an important link between the Atlantic and the Mediterranean.

## Conclusion

Tangier City is situated within a context marked by strong population growth, intense urbanization, and significant economic and touristic development. This urbanization is accompanied by peri-urbanization, and urban sprawl, leading to real estate developments that, to some extent, occur in a disorderly and uncontrolled manner. Given Tangier's coastal location, this rapid urbanization and densification of the coastline inevitably lead to increased pressures on the coastal area and associated challenges that need to be addressed. Throughout this study, we capitalized on freely available multi-source and multi-date remote sensing data, as well as GIS tools, notably on Google Earth Engine, to map artificialized surfaces. The primary objective

was to gain a better understanding of the spatiotemporal evolution of land reclaimed from the sea and its designated usage. The results obtained through the supervised classification of Landsat images using the random forest algorithm on the GEE platform, combined with the use of indicators (MNDWI, NDVI) during sampling, yielded highly satisfactory outcomes. The high values obtained for classification accuracies and Kappa coefficients have significantly minimized the risk of confusion between land use classes that are spectrally similar despite belonging to two different environments.

These results affirm substantial changes in land use in the Tangier region over 23 years (from 2000 to 2023), indicating significant urban expansion, notably in coastal areas. To better comprehend the evolution of land use changes, we compared the areas occupied by each class in 2000, 2008, 2015, and 2023. The spatiotemporal evolution of land reclaimed from the sea and its designated usage was analyzed during three periods: 2000–2008, 2008–2015, and 2015–2023. These results were complemented by statistical calculations of coastal change rates. According to the findings, the analyzed classes can be grouped into two categories. The first category demonstrates surface gains over time, especially the artificialized zones and forest classes, with their areas increasing by 8% from 2000–2008 to 2015–2023, followed by continental waters, which occupied 7% of the total studied area in 2015–2023, compared with 3% in 2000–2008. The second category consists of classes experiencing surface loss, namely bare soils and vegetation, which successively lost 12% and 8% of their surface.

Monitoring urbanization over these 23 years reveals that the city has expanded at the expense of the coastal area, covering an area of approximately 30.03 $km^2$ since 2000. In 2023, urban areas along the Tangier coastline account for 15%, primarily concentrated on sandy shores.

## References

Ait Brahim L., Bousta M., Jemmah I. A., El Hamdouni I., ElMahsani A., Abdelouafi A., Sossey Alaoui F., and Lallout I. (2018) Landslide susceptibility mapping using AHP method and GIS in the peninsula of Tangier (Rif-northern Morocco). MATEC Web of Conferences 149: 02084. Available at: https://doi.org/10.1051/matecconf/201814902084

Amani M., Ghorbanian A., Ahmadi S. A., Kakooei M., Moghimi A., Mirmazloumi S. M., Moghaddam S. H. A., Mahdavi S., Ghahremanloo M., Parsian S., Wu Q., and Brisco B. (2020) Google Earth Engine Cloud Computing Platform for Remote Sensing Big Data Applications: A Comprehensive Review. IEEE Journal of Selected Topics in Applied Earth Observations and Remote Sensing 13: 5326-5350. Available at: https://doi.org/10.1109/JSTARS.2020.3021052

Amini S., Saber M., Rabiei-Dastjerdi H., and Homayouni S. (2022) Urban Land Use and Land Cover Change Analysis Using Random Forest Classification of Landsat Time Series. Remote Sensing 14(11): 2654. Available at: https://doi.org/10.3390/rs14112654

Becker W. R., Ló T. B., Johann J. A., and Mercante E. (2021) Statistical features for land use and land cover classification in Google Earth Engine. Remote Sensing Applications: Society and Environment 21: 100459. Available at: https://doi.org/10.1016/j.rsase.2020.100459

Belgiu M., and Drăguț L. (2016) Random Forest in remote sensing: A review of applications and future directions. ISPRS Journal of Photogrammetry and Remote Sensing 114: 24-31. Available at: https://doi.org/10.1016/j.isprsjprs.2016.01.011

Betts M. G., Franklin S. E., and Taylor R. G. (2003) Interpretation of landscape pattern and habitat change for local indicator species using satellite imagery and geographic information system data in New Brunswick, Canada. Canadian Journal of Forest Research 33(10): 1821-1831. Available at: https://doi.org/10.1139/x03-104

Bourgoin C., Oszwald J., Bourgoin J., Gond V., Blanc L., Dessard H., Phan T. V., Sist P., Läderach P., and Reymondin L. (2020) Assessing the ecological vulnerability of forest landscape to agricultural frontier expansion in the Central Highlands of Vietnam. International Journal of Applied Earth Observation and Geoinformation 84: 101958. Available at: https://doi.org/10.1016/j.jag.2019.101958

Camalan S., Cui K., Pauca V. P., Alqahtani S., Silman M., Chan R., Plemmons R. J., Dethier E. N., Fernandez L. E., and Lutz D. A. (2022) Change Detection of Amazonian Alluvial Gold Mining Using Deep Learning and Sentinel-2 Imagery. Remote Sensing 14(7): 1746. Available at: https://doi.org/10.3390/rs14071746

Cheng G., Han J., and Lu X. (2017) Remote Sensing Image Scene Classification: Benchmark and State of the Art. Proceedings of the IEEE 105(10): 1865-1883. Available at: https://doi.org/10.1109/JPROC.2017.2675998

Dhu T., Giuliani G., Juárez J., Kavvada A., Killough B., Merodio P., Minchin S., and Ramage S. (2019). National Open Data Cubes and Their Contribution to Country-Level Development Policies and Practices. Data 4(4): 144. Available at: https://doi.org/10.3390/data4040144

Foody G. M. (2002) Status of land cover classification accuracy assessment. Remote Sensing of Environment 80(1): 185-201. Available at: https://doi.org/10.1016/S0034-4257(01)00295-4

Gillanders S. N., Coops N. C., Wulder M. A., Gergel S. E., and Nelson T. (2008) Multitemporal remote sensing of landscape dynamics and pattern change: Describing natural and anthropogenic trends. Progress in Physical Geography: Earth and Environment 32(5): 503-528. Available at: https://doi.org/10.1177/0309133308098363

Gislason P. O., Benediktsson J. A., and Sveinsson J. R. (2006) Random Forests for land cover classification. Pattern Recognition Letters 27(4): 294-300. Available at: https://doi.org/10.1016/j.patrec.2005.08.011

Gorelick N., Hancher M., Dixon M., Ilyushchenko S., Thau D., and Moore R. (2017) Google Earth Engine: Planetary-scale geospatial analysis for everyone. Remote Sens Environ 202: 18-27. Available at: https://doi.org/10.1016/j.rse.2017.06.031

Griffith J. A., Stehman S. V., Sohl T. L., and Loveland T. R. (2003) Detecting trends in landscape pattern metrics over 20 years using a sampling-based monitoring program. International Journal of Remote Sensing 24(1): 175-181. Available at: https://doi.org/10.1080/01431160305009

Hmamou M., and Bounakaya B. (2020) The Role of Artificial Impoundments in Improving Agricultural Production in The Semi-Arid Regions of Northern Morocco. Geography Environment, Sustainability 13(4): 32-42. Available at: https://doi.org/10.24057/2071-9388-2020-46

Huang S., Tang L., Hupy J. P., Wang Y., and Shao G. (2021) A commentary review on the use of normalized difference vegetation index (NDVI) in the era of popular remote sensing. Journal of Forestry Research 32(1): 1-6. Available at: https://doi.org/10.1007/s11676-020-01155-1

Imane B., Khadija A., Rachid E. H., Abdeladim B., Mustapha M., and Mohammed A. (2019) Modeling the Spatial Distribution of Rainfall in the Tangier Area (Northern Morocco). In M. Ezziyyani (Ed.), Advanced Intelligent Systems for Sustainable Development (AI2SD'2018) 913: 1-12. Springer International Publishing. Available at: https://doi.org/10.1007/978-3-030-11881-5_1

Jaiswal R. K., Saxena R., and Mukherjee S. (1999) Application of remote sensing technology for land use/land cover change analysis. Journal of the Indian Society of Remote Sensing 27(2): 123-128. Available at: https://doi.org/10.1007/BF02990808

Jiang Z. (2007) Interpretation of the modified soil-adjusted vegetation index isolines in red-NIR reflectance space. Journal of Applied Remote Sensing 1(1), 013503. Available at: https://doi.org/10.1117/1.2709702

Kadri N., Jebari S., Augusseau X., Mahdhi N., Lestrelin G., and Berndtsson R. (2023) Analysis of Four Decades of Land Use and Land Cover Change in Semiarid Tunisia Using Google Earth Engine. Remote Sensing 15(13): 3257. Available at: https://doi.org/10.3390/rs15133257

Khatami R., Mountrakis G., and Stehman S. V. (2017) Mapping per-pixel predicted the accuracy of classified remote sensing images. Remote Sensing of Environment 191: 156-167. Available at: https://doi.org/10.1016/j.rse.2017.01.025

Kolli M. K., Opp C., Karthe D., and Groll M. (2020) Mapping of Major Land-Use Changes in the Kolleru Lake Freshwater Ecosystem by Using Landsat Satellite Images in Google Earth Engine. Water 12(9): 2493. Available at: https://doi.org/10.3390/w12092493

Lambin E. F., Turner B. L., Geist H. J., Agbola S. B., Angelsen A., Bruce J. W., Coomes O. T., Dirzo R., Fischer G., Folke C., George P. S., Homewoo, K., Imbernon J., Leemans R., Li X., Moran E. F., Mortimore M., Ramakrishnan P. S., Richards J. F., Skanes H., Steffen W., Stone G. D., Svedin U., Veldkamp T. A., Vogel C., and Xu J. (2001) The causes of land-use and land-cover change: Moving beyond the myths. Global Environmental Change 11(4): 261-269. Available at: https://doi.org/10.1016/S0959-3780(01)00007-3

Liu C., Frazier P., and Kumar L. (2007) Comparative assessment of the measures of thematic classification accuracy. Remote Sensing of Environment 107(4): 606-616. Available at: https://doi.org/10.1016/j.rse.2006.10.010

Lu D., Mausel P., Batistella M., and Moran E. (2005) Land-cover binary change detection methods for use in the moist tropical region of the Amazon: A comparative study. International Journal of Remote Sensing 26(1): 101-114. Available at: https://doi.org/10.1080/01431160410001720748

Mamouni A., Moutchou B. E., and Fadel L. E. (2019) Apport de l'analyse géomorphologique dans l'étude de la fracturation de surface dans la région de Tanger (NW du Maroc) [Contribution of geomorphological analysis in the study of surface fracturing in the Tangier region (NW of Morocco)]. International Journal of Innovation and Scientific Research 41(2): 46-62 (in French).

Mas J. F. (2000) Une revue des méthodes et des techniques de télédétection du changement [A review of methods and techniques for remote sensing of change]. Canadian Journal of Remote Sensing, 26(4), 349-362. Available at: https://doi.org/10.1080/07038992.2000.10874785 (in French).

Mousa B. G., Shu H., Freeshah M., and Tariq A. (2020) A Novel Scheme for Merging Active and Passive Satellite Soil Moisture Retrievals Based on Maximizing the Signal to Noise Ratio. Remote Sensing 12(22): 3804. Available at: https://doi.org/10.3390/rs12223804

Mushtaq F., Henry M., O'Brien C. D., Di Gregorio A., Jalal R., Latham J., Muchoney D., Hill C. T., Mosca N., Tefera M. G., Morteo K., Franceschini G., Ghosh A., Tchana E., and Chen Z. (2022) An International Library for Land Cover Legends: The Land Cover Legend Registry. Land 11(7): 1083. Available at: https://doi.org/10.3390/land11071083

Muttitanon W., and Tripathi N. K. (2005) Land use/land cover changes in the coastal zone of Ban Don Bay, Thailand using Landsat 5 TM data. International Journal of Remote Sensing 26(11): 2311-2323. Available at: https://doi.org/10.1080/01431160512331326666

Phan T. N., Kuch V., and Lehnert L. W. (2020) Land Cover Classification using Google Earth Engine and Random Forest Clas-

sifier-The Role of Image Composition. Remote Sensing 12(15): 2411. Available at: https://doi.org/10.3390/rs12152411

Rawat J. S., and Kumar M. (2015) Monitoring land use/cover change using remote sensing and GIS techniques: A case study of Hawalbagh block, district Almora, Uttarakhand, India. The Egyptian Journal of Remote Sensing and Space Science, 18(1): 77-84. Available at: https://doi.org/10.1016/j.ejrs.2015.02.002

Reis S., Nişnci R., Uzun B., Yalçin A., Inan H., and Yomralioğlu T. (2003) Monitoring Land-Use Changes by GIS and Remote Sensing Techniques: Case Study of Trabzon.

Rodriguez-Galiano V. F., Ghimire B., Rogan J., Chica-Olmo M., and Rigol-Sanchez J. P. (2012) An assessment of the effectiveness of a random forest classifier for land-cover classification. ISPRS Journal of Photogrammetry and Remote Sensing 67: 93-104. Available at: https://doi.org/10.1016/j.isprsjprs.2011.11.002

Sbai A., Lasgaa H., and Mohammed U. (2016) Contribution de la télédétection dans l'étude et l'évolution spatiotemporelle du couvert végétal: Cas du couloir de Taourirt - El Aioun et ses bordures montagneuses (Maroc oriental) [Contribution of remote sensing in the study and spatiotemporal evolution of plant cover: Case of the Taourirt - El Aioun corridor and its mountainous borders (eastern Morocco)] (in French).

Setti S., Maheswaran R., Radha D., Sridhar V., Barik K. K., and Narasimham M. L. (2020) Attribution of Hydrologic Changes in a Tropical River Basin to Rainfall Variability and Land-Use Change: Case Study from India. Journal of Hydrologic Engineering 25(8): 05020015. Available at: https://doi.org/10.1061/(ASCE)HE.1943-5584.0001937

Sharma R., and Joshi P. K. (2013) Monitoring Urban Landscape Dynamics Over Delhi (India) Using Remote Sensing (1998-2011) Inputs. Journal of the Indian Society of Remote Sensing, 41(3), 641-650. Available at: https://doi.org/10.1007/s12524-012-0248-x

Srivastava R., Tiwari A., and Giri V. (2019) Solar radiation forecasting using MARS, CART, M5, and random forest model: A case study for India. Heliyon 5: e02692. https://doi.org/10.1016/j.heliyon.2019.e02692

Singh A. (1989) Review Article Digital change detection techniques using remotely sensed data. International Journal of Remote Sensing 10(6): 989-1003. Available at: https://doi.org/10.1080/01431168908903939

Tatsumi K., Yamashiki Y., Canales Torres M. A., and Taipe C. L. R. (2015) Crop classification of upland fields using Random Forest of time-series Landsat 7 ETM+ data. Computers and Electronics in Agriculture 115: 171-179. Available at: https://doi.org/10.1016/j.compag.2015.05.001

Wahbi M., Boulaassal H., Maatouk M., El Kharki O., and Yazidi Alaoui O. (2020) Monitoring the Urban Sprawl of the City of Tangier from Spot and Sentinel2 Images. In Advanced Intelligent Systems for Sustainable Development (AI2SD'2019) Volume 3-Advanced Intelligent Systems for Sustainable Development Applied to Environment, Industry and Economy (pp. 453-465). Springer International Publishing. Available at: https://doi.org/10.1007/978-3-030-36671-1_40

Xu H. (2008) A new index for delineating built-up land features in satellite imagery. International Journal of Remote Sensing 29(14): 4269-4276. https://doi.org/10.1080/01431160802039957

Yuan F., Sawaya K. E., Loeffelholz B. C., and Bauer M. E. (2005) Land cover classification and change analysis of the Twin Cities (Minnesota) Metropolitan Area by multitemporal Landsat remote sensing. Remote Sensing of Environment 98(2-3): 317-328. Available at: https://doi.org/10.1016/j.rse.2005.08.006

Zeferino L. B., Souza L. F. T. D., Amaral C. H. D., Fernandes Filho E. I., and Oliveira T. S. D. (2020) Does environmental data increase the accuracy of land use and land cover classification? International Journal of Applied Earth Observation and Geoinformation 91: 102128. Available at: https://doi.org/10.1016/j.jag.2020.102128

Zha Y., Gao J., and Ni S. (2003) Use of normalized difference built-up index in automatically mapping urban areas from TM imagery. International Journal of Remote Sensing 24(3): 583-594. Available at: https://doi.org/10.1080/01431160304987